

# The vertical structure of Jupiter’s equatorial zonal wind above the cloud deck, derived using mesoscale gravity waves

C. Watkins<sup>1</sup> and J. Y-K. Cho<sup>1</sup>

Data from the Galileo Probe, collected during its descent into Jupiter’s atmosphere, is used to obtain a vertical profile of the zonal wind from  $\sim 0.5$  bar (upper troposphere) to  $\sim 0.1$   $\mu$ bar (lower thermosphere) at the probe entry site. This is accomplished by constructing a map of gravity wave Lomb-Scargle periodograms as a function of altitude. The profile obtained from the map indicates that the wind speed above the visible cloud deck increases with height to  $\sim 150$   $\text{m s}^{-1}$  and then levels off at this value over a broad altitude range. The location of the turbopause, as a region of wide wave spectrum, is also identified from the map. In addition, a cross-equatorial oscillation of a jet, which has previously been linked to the quasi-quadrennial oscillation in the stratosphere, is suggested by the profile.

## 1. Introduction

The horizontal structure of Jupiter’s zonal (east-west) winds at the level of the visible cloud deck on Jupiter have been observed for many decades [e.g., *Limaye*, 1986; *Ingersoll*, 2004; *García-Melendo and Sánchez Lavega*, 2001; *Vasavada and Showman*, 2005; *Li et al.*, 2006]. In contrast, the vertical structure of zonal winds is not well known – especially away from the cloud deck and in the equatorial region. This is because of the lack of usable tracers and the breakdown of the thermal wind relation near the equator, preventing latitudinal temperature measurements to be related to the vertical wind shear.

In December 1995 the Galileo probe entered Jupiter’s upper atmosphere at  $6^\circ$  N, above a  $5\mu\text{m}$  hot spot in the north equatorial belt. During the descent the Atmospheric Structure Instrument on board collected information about the density, pressure, and temperature of the atmosphere [*Seiff et al.*, 1998]. Analysis of the temperature profile in the thermospheric and stratospheric regions identified discernible perturbations which have been interpreted as manifestations of internal, or vertically propagating, gravity waves [*Young et al.*, 1997, 2005; *Matcheva and Strobel*, 1999]. Vertical temperature profiles for Jupiter’s atmosphere have also been obtained from occultation studies using stars and other spacecraft. A number of these profiles contain oscillations that have been characterised as manifestations of internal gravity waves as well [*French and Gierasch*, 1974; *Lindal*, 1992; *Hubbard et al.*, 1995; *Raynaud et al.*, 2003, 2004].

Gravity waves are oscillations of fluid parcels about their altitudes of neutral buoyancy [*Gossard*, 1975]. The waves are a common feature of stably stratified atmospheres. They have been captured in images of Jupiter’s clouds, typically

near the planet’s equator [*Flasar and Gierasch*, 1986; *Arregi et al.*, 2009; *Reuter et al.*, 2007]. Fig. 1 shows an example. Internal gravity waves (hereafter simply gravity waves) grow in amplitude, due to the fall in background atmospheric density. The dynamics of such waves is described by the Taylor–Goldstein equation [*Taylor*, 1931; *Goldstein*, 1931],

$$\frac{d^2 w}{dz^2} + m^2(z) w = F(z). \quad (1)$$

Here  $w$  is the perturbation in the vertical wind, which is adjusted for the amplitude growth and also assumed to be oscillatory (wave-like) in the horizontal direction and time;  $F$  is a function that represents the source and dissipation of waves; and,  $m$  is the vertical wavenumber, which depends on the physical properties of the medium in which the waves propagate. Specifically,

$$m(z) = \left[ \frac{N^2}{I^2} - \frac{1}{I} \frac{d^2 I}{dz^2} - \frac{1}{HI} \frac{dI}{dz} - \frac{1}{4H^2} \left( 1 - 2 \frac{dH}{dz} \right) - k^2 \right]^{1/2}, \quad (2)$$

where  $N$  is the Brunt–Väisälä (buoyancy) frequency;  $I$  is the intrinsic phase speed,  $c - u_0$ , where  $c$  is the horizontal phase speed and  $u_0$  is the zonal wind;  $H$  is the density scale height; and,  $k$  is the horizontal wavenumber. In general, all of the variables depend on altitude  $z$ . Crucially, the zonal wind profile  $u_0(z)$  can be obtained by solving for  $I = I(H, k, N, m)$  in equation (2). In this letter we present a profile from this inversion that span much larger range of altitude above the 1 bar level (range of  $\sim 500$  km) than in past analyses.

## 2. Method

For the inversion we compute  $H$  from the collected density profile. We also use  $k = 2\pi/300$   $\text{km}^{-1}$  from the average value obtained in analysis of Voyager images [*Flasar and Gierasch*, 1986]. Other analyses have reported slightly different values (e.g., average of  $2\pi/165$   $\text{km}^{-1}$  by *Arregi et al.* [2009]); however, as long as  $k^2 \ll m^2$  (as is the case here), the value of  $k$  does not significantly alter the result of the inversion.  $N$  and  $m$  are obtained from the potential temperature,  $\theta = T(p_{\text{ref}}/p)^\kappa$ , related to specific entropy of the atmosphere; here  $T$  is the temperature,  $p$  is the pressure,  $p_{\text{ref}} = 1$  bar is a constant reference pressure and  $\kappa = R/c_p$  with  $R$  the specific gas constant and  $c_p$  the specific heat at constant pressure. To obtain  $N$  and  $m$ , we decompose  $\theta$  into a mean background  $\bar{\theta}$  (extracted using a spatially-moving fitting window) and a small perturbation  $\Delta\theta$  about the mean (presumed caused by mesoscale gravity waves). Such decomposition of temperature is standard in gravity wave studies [*Lindzen*, 1990; *Nappo*, 2002; *Young et al.*, 1997], and is reasonable here given that the spatial scales of the background and waves are well separated. Further, the horizontal distance travelled by the probe in the region studied, 3300 km, is small compared to Jupiter’s circumference and is completely within the hot-spot entered by probe [*Orton et al.*,

<sup>1</sup>School of Physics and Astronomy, Queen Mary University of London, London, UK.

1998]; hence, zonal variation in the background over this distance is not expected to be significant.

Fig. 2a shows the relative perturbation,  $\Delta\theta/\bar{\theta}$ , resulting from a 75 km- wide moving window. We have checked that the result is not affected by the choice of window size, by varying the size from 55 km to 85 km. Fig. 2b shows  $N = [g d(\ln\bar{\theta})/dz]^{1/2}$  resulting from the decomposition; here  $g = g(z)$  is the gravity. In the figure note that  $N$  is much smaller in the region below  $\sim 20$  km than that above (the stratosphere)—in agreement with *Magalhães et al.* [2002], whose observations give  $N \approx 6 \times 10^{-3} \text{ s}^{-1}$  in the lower region. This represents a possible ducting region, a source for the waves in the probe data.

Although  $w$  information was not collected by the probe,  $m(z)$  can still be obtained from  $\Delta\theta$  through the polarization relation [e.g., *Watkins and Cho*, 2010]. For this we generate a series of Lomb-Scargle periodograms [*Scargle*, 1982] of the  $\Delta\theta$  data, which is non-uniformly spaced in  $z$ . The non-uniform spacing renders analysis by standard Fourier or wavelet transforms unsuitable. One periodogram at each  $z$  is generated using a smoothing window. We have also verified in this procedure that the obtained result varies little between different sized smoothing windows. All the periodograms are subsequently combined to produce a two-dimensional map of the wave spectral energy density as a function of wavenumber and altitude,  $\mathcal{E} = \mathcal{E}(m^*, z)$ , shown in Fig. 3; here  $m^*$  is the vertical wavenumber  $m$  prior to an adjustment for wave propagation geometry. Before discussing this adjustment, we discuss three features which are already apparent in the  $\mathcal{E}$  map.

### 3. Results

First, gravity waves identified previously [*Young et al.*, 2005] are recovered (W1 and W2 in the map). This agreement gives confidence in our procedure. In addition to those waves, we identify in our analysis new gravity waves throughout the analyzed domain. In particular, note the high energy density (dark red) regions near the 50 km, 300 km and 400 km altitudes all with  $m^* \approx 0.25$ . These constitute new waves.

Second, we identify a region consistent with a turbopause  $\sim 50$  km thick, centered at approximately 400 km altitude. This is the region where the width of the sub-spectrum containing significant energy increases markedly. In this region, molecular diffusion becomes comparable to eddy diffusion and gravity waves—growing in amplitude as they propagate upward—break, transferring energy into the higher wavenumbers. Above this region, energy is lower across the entire spectrum and the spectrum itself is much steeper (i.e., narrower) than that for the turbopause region. Above the turbopause region, the atmosphere becomes inhomogeneous, separating out into layers of different molecular species. Past studies have placed Jupiter's turbopause at the  $\sim 5\mu\text{bar}$  [*Festou et al.*, 1981] and  $\sim 0.5\mu\text{bar}$  [*Yelle et al.*, 1996] levels, based on observations and modeling. Our result supports the latter location.

Third, in the lower part of the analyzed domain there appears to be a ducting region, a region with a sharp jump in  $N$ . As already noted, such a region can serve as a source of gravity waves. Horizontally propagating gravity waves in this region have previously been observed (see, e.g., Fig. 1), which have been suggested as waves trapped in a “leaky” duct. The ducted wave travels horizontally by undergoing internal reflections at the boundaries; however, part of the wave escapes the duct to propagate vertically. Because the wavenumber with maximum energy in the  $\mathcal{E}$  map can be traced down to the ducting region, it is likely that the waves have come from there.

Note that above the ducting region the number of local peaks in the spectrum generally reduces with altitude (the

centroid of the spectrum at each height is shifted to lower wavenumber). Also, the magnitude of the peak energy in the low wavenumber (white line in Fig. 3) is high at first, then decreases, and then increases again along the white line, until the topside of the turbopause region at  $\sim 425$  km above the 1 bar level. This is indicative of wave saturation or encounters with a critical layer, where  $I = 0$  locally, for high number wavenumbers as they propagate upward. The second or third multi-peaked altitude regions, between  $\sim 200$  km and  $\sim 300$  km above the 1 bar level, may be due to wave breaking and secondary wave generation from breaking layers.

As alluded to earlier,  $m^*$  differs from the required wavenumber  $m$ . The latter is the wavenumber that would be observed by a probe travelling in a vertical direction. However, throughout most of its entry phase, the probe had a shallow angle of attack ( $\sim 7^\circ$  below the horizontal), which changes the wavenumber observed by the probe during its passage in the upper part of the analyzed domain. We use the geometry of the probe's path to obtain the true vertical wavenumber,

$$m = \left( \frac{\tan \gamma \tan \beta}{1 - \tan \gamma \tan \beta} \right) m^*, \quad (3)$$

where  $\gamma$  is the angle of attack and  $\beta$  is the angle the wavevector makes with the horizontal. We make no correction for the relative motion of the probe with respect to the wave since the probe's velocity is supersonic (indeed, hypersonic, with up to Mach 51) for much of the entry phase. Gravity wave phase speeds are subsonic.

Although  $\gamma = \gamma(z)$  is known from the probe's trajectory [*Seiff et al.*, 1998],  $\beta$  is not. To estimate this quantity, we assume that the probe's trajectory is vertical in the period just before parachute deployment. This is not far from the actual situation since the probe's angle of attack was  $83^\circ$  just before the parachute was deployed, near the lower boundary of our domain. In this region,  $m^* \approx m$ ; and, since

$$\beta = \arccos \left( \frac{k}{\sqrt{k^2 + m^2}} \right), \quad (4)$$

we have  $\beta \approx 85^\circ$ . Also, in this region  $m \approx 0.25 \text{ km}^{-1}$  (giving vertical wavelength of  $\approx 25$  km), in good agreement with previously recovered values [*Magalhães et al.*, 2002; *Arregi et al.*, 2009]. Now, all the parameters required to recover  $I$  have been obtained, and a vertical profile for  $I$  can be estimated.

Finally, to obtain  $u_0$  from  $I$  a value for the horizontal phase speed  $c$  is required. This is not well known. However, equatorial gravity waves with a phase speed of about  $100 \text{ m s}^{-1}$  greater than the winds have been observed in images of Jupiter's clouds returned by New Horizons [*Reuter et al.*, 2007]. This gives  $c \approx 180 \text{ m s}^{-1}$ . The Doppler Wind Experiment (DWE) on the probe has measured the zonal winds to be approximately this speed in the deeper atmosphere [*Atkinson et al.*, 1998], suggesting that the waves could have been driven by convective overshoot below the clouds. This value also agrees well with the 140–195  $\text{m s}^{-1}$  range reported for the similar region, at the probe entry site [*Magalhães et al.*, 2002]. Somewhat smaller values (approximately 70–145  $\text{m s}^{-1}$ ) have been obtained for waves at different longitudes [*Arregi et al.*, 2009]. Such variation in  $c$  does not change the shape of the  $u_0$  profile we recover, but the magnitude would be reduced. Variations of  $c$  with altitude would increase the uncertainty as well, but they are expected to be small and not fundamentally change the profile. This gives the profile for  $u_0(z)$  shown in Fig. 4a. Here we have used  $c = 180 \text{ m s}^{-1}$ . The standard deviation shown indicates the variation in the profile given by the various smoothing window sizes considered in constructing  $\mathcal{E}$ .

## 4. Discussion

The DWE reported flow speeds that increase with depth reaching  $170 \text{ m s}^{-1}$  at the 5 bar level and then remaining high at lower levels [Atkinson *et al.*, 1998]. The upper part of the DWE profile is shown in Fig. 4a. The wind speed at the bottom of our profile agrees well with that at the top of the DWE profile. Our profile shows increasing zonal wind speed with altitude (up to  $\sim 100 \text{ km}$  above the 1 bar level). This implies that the wind speed is a minimum near the cloud-top level. This is similar to what has been observed from studies using the thermal wind equation [Flasar *et al.*, 2004; Simon-Miller *et al.*, 2006]. However, in our profile this high speed wind is not a jet, as the zonal wind speed does not diminish appreciably with altitude near this level. In fact, the speed is roughly constant throughout the stratosphere, starting from this level. There are some fluctuations of the order of  $20 \text{ m s}^{-1}$  in the wind speed in the thermosphere. The Richardson number,  $Ri = N^2 (du_0/dz)^{-2}$ , is greater than  $1/4$  for the entire profile, which indicates the flow is stable with respect to Kelvin-Helmholtz instability.

Temporal variations in the temperature profile of Jupiter's equatorial stratosphere have been observed to have a period of 4 to 5 years and are therefore known as the quasi-quadrennial oscillation (QO) [Leovy *et al.*, 1991; Friedson, 1999]. These oscillations have been linked to variations in the zonal wind observed via cloud-tracking on Jupiter with a period of  $\sim 4.4$  years [Simon-Miller *et al.*, 2007]. Further, a jet located just north of the equator, derived using the thermal wind equation applied to data gathered in December 2000 and January 2001, has been linked to the QO [Flasar *et al.*, 2004]. A jet of similar magnitude, just south of the equator, has been observed in observations gathered in 1979 [Simon-Miller *et al.*, 2006] (which fits well with a period of 4.4 years), suggesting this jet may be oscillating about the equator. No such jet is visible in our profile. However, the probe entered Jupiter's atmosphere 5 years before the northern jet was observed. Thus, our profile is consistent with such an oscillation as the jet would be located south of the equator, away from the probe entry site, at the time the probe entered.

Gravity wave creation and dissipation is associated with heating and cooling of the atmosphere. Ignoring molecular viscosity, which is only important above the turbopause, the heating rate is proportional to the vertical gradient of energy flux—specifically,

$$\frac{\partial T}{\partial t} = -\frac{1}{\rho c_p} \frac{\partial F_z}{\partial z} \quad (5)$$

We estimate the energy flux,  $F_z = \overline{\rho \phi w}$ , from  $\Delta\theta$  using the polarization relations to derive the perturbations in the geopotential  $\phi$  and the vertical velocity  $w$ . The flux comes from the zonal average of the product of these quantities. Since the product is not available to us we average over a single vertical wavelength instead. The heating rate profile thus obtained is shown in Fig 4b. It can be seen that heating is small through the stratosphere. Indeed, on average it is very close to zero. It is only in the thermosphere that the average heating rate deviates from zero with a magnitude of  $\sim 0.5 \text{ K}$  per Jupiter rotation. The flux responsible for heating in this region is small ( $F_z < 10^{-3} \text{ W m}^{-2}$ ), compared to radiation fluxes measured in the troposphere ( $3 < F_z < 16 \text{ W m}^{-2}$ ) [Sromovsky *et al.*, 1998]. Nevertheless, the peak heating rate magnitude is about 50 times larger, partly because the lower thermosphere is much less dense than the troposphere.

The circulation of Jupiter's stratosphere is important for understanding the planet's circulation as a whole. The location of the turbopause is essential for understanding the coupling between Jupiter's upper atmosphere and the circulation in the lower atmosphere. The Juno mission will

explore the troposphere of Jupiter to depths of 100 bar or more. This will provide better insight to the source and behaviour of gravity waves in the troposphere, possibly allowing better limits to be derived for the wave-vector angle  $\beta$  in our analysis and better understanding of the mechanisms that generate the gravity waves. The planned Jupiter Icy Moon Explorer (JUICE) mission will directly study gravity wave activity and zonal winds in the stratosphere of Jupiter, extending the result present here.

**Acknowledgments.** C.W. is supported by the Science and Technology Facilities Council (STFC), and J.Y.-K.C. is supported by the STFC PP/E001858/1 grant. The authors acknowledge H. Thrastarson, I. Polichtchouk, and C. Agnor for useful discussions. We thank the reviewers for helpful suggestions.

## References

- Arregi, J., J. F. Rojas, R. Hueso, and A. Sánchez-Lavega, (2009), Gravity waves in Jupiters equatorial clouds observed by the Galileo orbiter, *Icarus*, 202, 358–360.
- Atkinson, D. H., J. B. Pollack, and A. Seiff, (1998), The Galileo Probe Doppler Wind Experiment: measurement of the deep zonal winds on Jupiter, *J. Geophys. Res.*, 103, 22911–22928.
- Festou, M. C. et al. (1981), Composition and Thermal Profiles of the Jovian Upper Atmosphere Determined by the Voyager Ultraviolet Stellar Occultation Experiment. *J. Geophys. Res.*, 86, 5715–5725.
- Flasar, F. M. and, P. J. Gierasch, (1986) Mesoscale Waves as a Probe of Jupiters Deep Atmosphere, *J. Atmos. Sci.*, 43, 2683–2707.
- Flasar, F. M. *et al.*, (2004), An intense stratospheric jet on Jupiter, *Nature*, 427, 132–135.
- French, R. G., and P. J. Gierasch, (1974), Waves in the Jovian upper atmosphere, *J. Atmos. Sci.*, 31, 1707–1712.
- Friedson, A.J., (1999), New Observations and Modelling of a QBO-Like Oscillation in Jupiter's Stratosphere, *Icarus*, 137, 34–55.
- García-Melendo E., and A. Sánchez Lavega, (2001), A Study of the Stability of Jovian Zonal Winds from HST Images: 1995–2000, *Icarus*, 152, 316–330.
- Goldstein, S., (1931), On the Stability of Superposed Streams of Fluids of Different Densities, *Proc. of the R. Soc. A*, 132, 524–548.
- Gossard, E. E., and W. H. Hooke, (1975), *Waves in the Atmosphere*, Elsevier, Amsterdam, Netherlands.
- Hubbard, W.B., V. Haemmerle, C. C. Porco, G. H. Rieke, and M. J. Reike, (1995) The Occultation of SAO 78505 by Jupiter, *Icarus*, 113, 103–109.
- Ingersoll, A. P., et al. (2004) , in *Jupiter: The Planet, Satellites and Magnetosphere* edited by F. Bagenal et al., pp. 105–128, Cambridge University Press, Cambridge, UK.
- Leovy, C. B., A. J. Friedson, and G. S. Orton, (1991), The quasi-quadrennial oscillation of Jupiter's equatorial stratosphere, *Nature*, 354, 380–382.
- Li, L. *et al.*, (2006) Vertical wind shear on Jupiter from Cassini images. *J. Geophys. Res.* 111, E0400401–E0400411.
- Limaye, S. S., (1992), Jupiter: New estimates of the mean zonal flow at the cloud level, *Icarus*, 65, 335–352.
- Lindal, G. F., (1992), The Atmosphere of Neptune: An Analysis of Radio Occultation Data Acquired with Voyager 2, *Astrophys. J.*, 103, 967–982.
- Lindzen, R. S. (1990) *Dynamics in Atmospheric Physics*, Cambridge University Press, Cambridge, UK.
- Magalhães, J. A., A. Seiff and R. E. Young (2002), The Stratification of Jupiters Troposphere at the Galileo Probe Entry Site, *Icarus*, 158, 410–433.
- Matcheva, K. I., and D. F. Strobel (1999), Heating of Jupiter's Thermosphere by Dissipation of Gravity Waves Due to Molecular Viscosity and Heat Conduction, *Icarus*, 140, 328–340.

- Nappo, C. J., (2002), *An Introduction to Atmospheric Gravity Waves*, Elsevier Academic Press, San Diego, Calif.
- Orton, G. S. et al., (1998), Characteristics of the Galileo probe entry site from Earth-based remote sensing observations, *J. Geophys. Res.*, *103*, 22791–22814.
- Raynaud, E. et al., (2003), The 10 October 1999 HIP 9369 occultation by the northern polar region of Jupiter: ingress and egress lightcurves analysis, *Icarus*, *162*, 344–361.
- Raynaud, E., K. Matcheva, P. Drossart, F. Roques, and B. Sicardy, (2004), A re-analysis of the 1971 Beta Scorpii occultation by Jupiter: study of temperature fluctuations and detection of wave activity, *Icarus*, *168*, 324–335 (2004).
- Reuter, D.C. et al., (2007), Jupiter Cloud Composition, Stratification, Convection, and Wave Motion: A View from New Horizons. *Science*, *318*, 223–225.
- Scargle, J. D., (1982), Studies in astronomical time series analysis. II-Statistical aspects of spectral analysis of unevenly spaced data, *Astrophys. J.*, *263*, 835–853.
- Seiff, A. et al., (1998), Thermal structure of Jupiter's atmosphere near the edge of a 5- $\mu$ m hot spot in the north equatorial belt, *J. Geophys. Res.*, *103*, 22857–22889.
- Simon-Miller, A. A. et al. (2006) Jupiter's atmospheric temperatures: From Voyager IRIS to Cassini CIRS. *Icarus*, *180*, 98–112 (2006).
- Simon-Miller, A. A., B. W. Poston, G. Orton, and B. Fisher, (2007) Wind variations in Jupiter's equatorial atmosphere: A QO counterpart?, *Icarus*, *186*, 192–203.
- Sromovsky, A. et al., (1998), Galileo probe measurements of thermal and solar radiation fluxes in the Jovian atmosphere, *J. Geophys. Res.*, *103*, 22929–22977.
- Taylor, G.I., (1931), Effect of Variation in Density on the Stability of Superposed Streams of Fluid, *Proc. of the R. Soc. A*, *132*, 499–523.
- Vasavada, A. R. and A. P. Showman, (2005), Jovian atmospheric dynamics: an update after Galileo and Cassini, *Rep. Prog. Phys.*, *68*, 1935–1996.
- Watkins, C., and J. Y-K. Cho, (2010) Gravity waves on hot extrasolar planets. I. Propagation and interaction with the background. *Astrophys. J.*, *714*, 904–914.
- Yelle, R.V. et al., (1996), Structure of Jupiters upper atmosphere: Predictions for Galileo, *J. Geophys. Res.*, *101*, 2149–2161.
- Young, L. A., R. V. Yelle, R. Young, A. Seiff, and D. B. Kirk, (1997), Gravity waves in Jupiter's thermosphere, *Science*, *276*, 108–111.
- Young, L.A., R. V. Yelle, R. Young, A. Seiff, and D. B. Kirk, (2005) Gravity waves in Jupiters stratosphere as measured by the Galileo ASI experiment, *Icarus*, *173*, 185–199.

---

J. Y-K. Cho, School of Physics and Astronomy, Queen Mary University of London, Mile End Road, London E1 4NS, UK. (J.Cho@qmul.ac.uk)

C. Watkins, School of Physics and Astronomy, Queen Mary University of London, Mile End Road, London E1 4NS, UK. (C.Watkins@qmul.ac.uk)

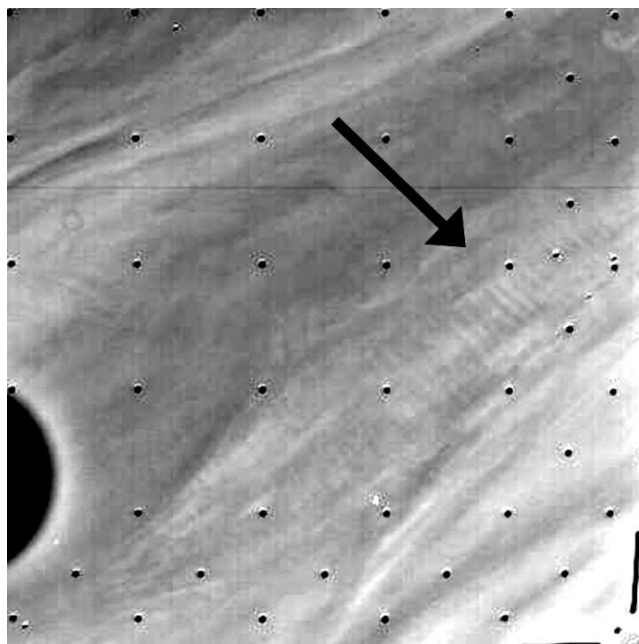


**Figure 1.** Gravity wave in Jupiter's atmosphere (Voyager image 16316.34). This wave is propagating horizontally in the troposphere. Many such waves are captured in the Voyager images [Flasar and Gierasch, 1986]. Image contrast has been enhanced to improve the visibility of the wave. The wave's location is indicated by the arrow. Image courtesy NASA/JPL-Caltech.

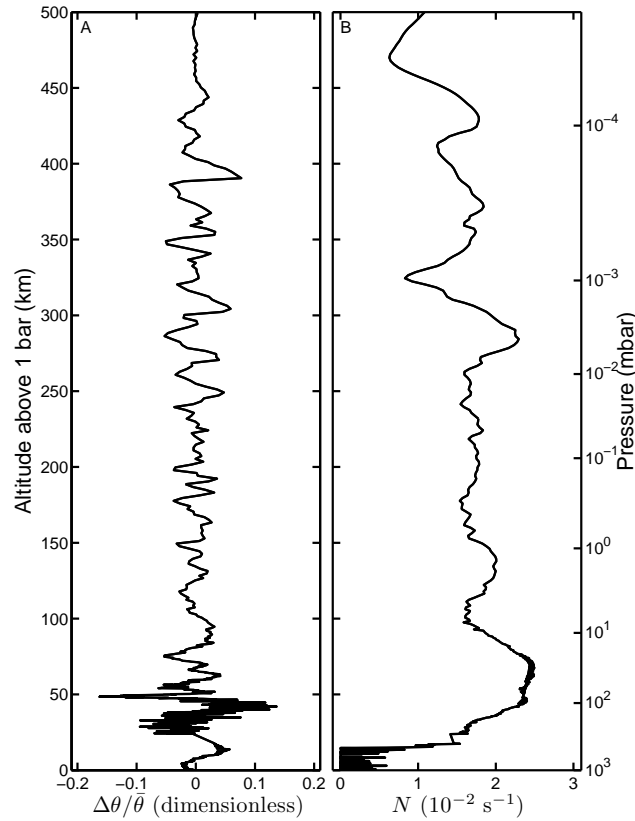


**Figure 2.** Relative potential temperature perturbation and Brunt-Väisälä (buoyancy) frequency profiles for Jupiter’s atmosphere. All altitudes are relative to the 1 bar pressure level. The profiles are based on data gathered from  $t = -173.055$  s to  $t = 218.170$  s;  $t = 0$  s is the point of parachute deployment. Our analysis used the complete set of acceleration data collected from both accelerometers with the exception of one outlier at  $t = -157.742$  s. The acceleration data collected by the probe includes a small spurious oscillation *Seiff et al.* [1998] which we did not smooth out as its effects on the calculation was negligible in the atmospheric region we analyzed. The bottom 25 km of the profile is from direct measurement of the temperature with the first 15 s of direct temperature measurements removed as these were anomalously high. **a**, The vertical profile of potential temperature perturbations,  $\Delta\theta$ , scaled by the background value,  $\theta$ . The perturbations show wavelike oscillations throughout the stratosphere and lower thermosphere. Note that the short wavelength oscillations in the layer between 25 km and 50 km are due to accelerations caused by buffeting of the probe as its velocity became subsonic. **b**, The Brunt-Väisälä frequency is the maximum frequency that a gravity wave can have and shows the stability of the atmosphere against convective stability.

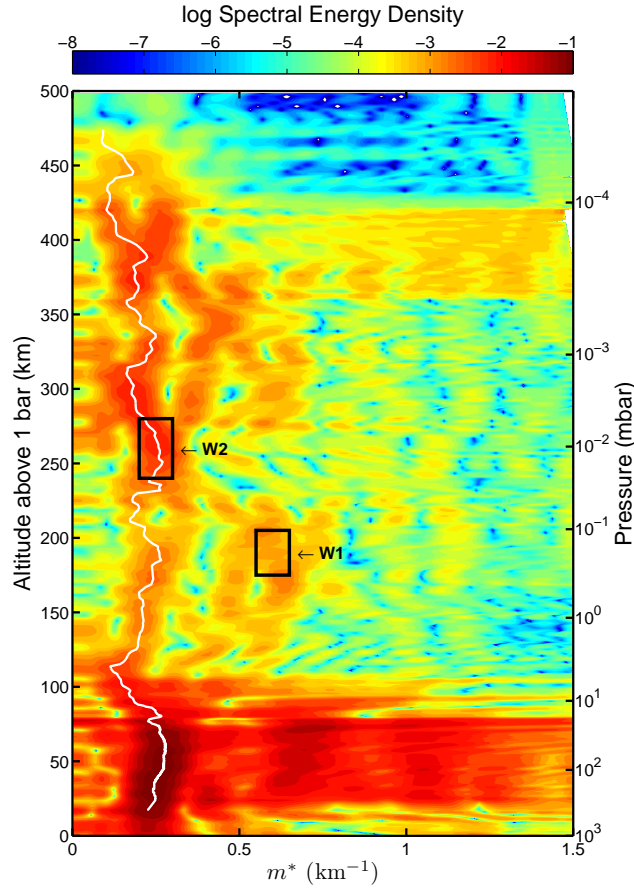


**Figure 3.** Moving Lomb-Scargle periodogram of the potential temperature perturbation from Fig. 2a. Regions of high spectral energy are in red while low energy is in blue. The variation of the observed vertical wavenumber  $m^*$  is shown (white line). The line is produced by identifying local energy maxima and constructing a line joining them, avoiding local minima, starting at the level of the duct in the troposphere. Note that there are other waves within the periodogram we do not consider in our analysis. One such wave, the region of high energy at  $m^* \approx 0.61 \text{ km}^{-1}$  between 180 km and 210 km altitude (labelled W1) has been previously identified as a saturating gravity wave *Young et al.* [2005]. Another region (labelled W2) has also been previously identified *Young et al.* [2005]. The region at an altitude of around 400 km shows a broadening of the range of wavenumbers with increased spectral energy. This is indicative of the turbopause, the region where waves break and the atmosphere begins to become heterogeneous.

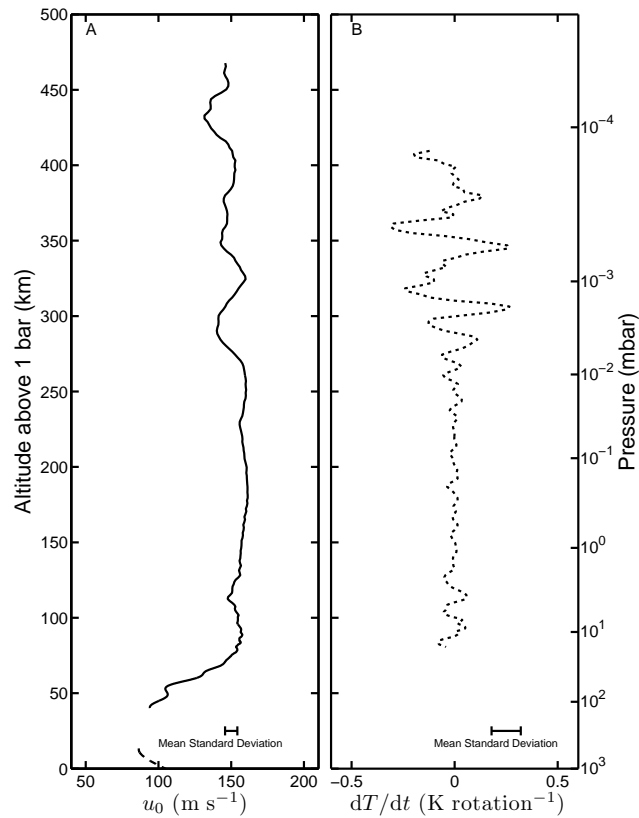


**Figure 4.** The vertical profiles of the background zonal wind speed  $u_0$  and heating rate,  $dT/dt$ . **a**, The zonal wind is shown (solid) with the average standard deviation of the variation across smoothing and periodogram windows indicated. The zonal speed profile found by the Doppler Wind Experiment is shown at the bottom (dashed) for comparison. **b**, The vertical profile of the heating rate is shown (dotted), as temperature change per Jovian rotation (9.925 h), with the average standard deviation of the variation across smoothing and periodogram windows indicated.